

Design Optimization and Experimental Study of Coreless Axial-flux PM Machines with Wave Winding PCB Stators

Peng Han^{1,*}, Senior Member, IEEE, Damien Lawhorn^{1,*}, Student Member, IEEE, Yaser Chulaee¹, Student Member, IEEE, Donovan Lewis¹, Student Member, IEEE, Greg Heins², Member, IEEE, and Dan M. Ionel¹, Fellow, IEEE

¹SPARK Lab, ECE Dept., University of Kentucky, Lexington, KY 40506, USA

²Regal Beloit Corporation, Australia, Rowville, VIC 3178, Australia

peng.han@ieee.org, damien.lawhorn@ieee.org, yaser.chulaee@uky.edu, donovin.lewis@uky.edu, greg.heins@ieee.org, dan.ionel@ieee.org

Abstract—This paper presents a systematic design optimization and experimental study of coreless axial-flux permanent magnet (AFPM) machines with wave winding printed circuit board (PCB) stators. Existing PCB winding configurations are briefly reviewed and compared to serve as a performance reference. A new concept—the “macro coil”—is proposed to model PCB stator windings in 3D finite element analysis (FEA) to facilitate large-scale multi-objective optimization with the winding eddy current losses evaluated in each design candidate. The detailed trace-by-trace model for a selected optimal design is then built to check the voltage difference between parallel paths and the resulting circulating currents. A prototype with two PM rotors and a central stator comprising multiple stacked PCBs has been fabricated and tested on a customized test fixture for experimental validation.

Index Terms—Axial-flux, coreless machines, FEA, multi-objective optimization, permanent-magnet machines.

I. INTRODUCTION

Axial-flux permanent-magnet (AFPM) synchronous machines have attracted much attention for a wide range of applications, such as heating, ventilation, and air conditioning (HVAC) systems, industrial motor drives, electric vehicles, aircraft propulsion, etc. Among all topology variants, the coreless type eliminates the magnetic cores and the associated core losses, resulting in potential simplifications of the manufacturing process, increased efficiency, and reduced weight and volume [1, 2].

In coreless AFPM machines, windings are directly exposed to the air-gap flux density variations without the protection of slots, so the cross-sectional dimensions of wires have to be minimized to suppress the induced eddy currents. Litz wires and printed circuit board (PCB) windings have been considered two promising options [3]. Litz wires consist of

multiple electrically-insulated strands with diameters no larger than AWG 38 wires. Litz wire strands are usually twisted or woven to minimize the skin effect and proximity effect. Compared to wired windings, the PCB windings have more design flexibility and are more suitable for integration with drives and controllers. Better heat dissipation capability, which enables higher current density, has been reported in [4, 5].

There are four main types of PCB winding patterns: the conventional distributed winding implemented by PCB traces [6, 7], the spiral winding [8–10] and its variants [11, 12], the progressive wave winding [5, 13], and the continuous wave winding [4], as illustrated in Fig. 1.

The conventional distributed winding implemented by PCB traces, relies heavily on the sophisticated design and implementation of radial conductors end connections. It is suitable for machines with low polarities. For example, the layout shown in Fig. 1a corresponds to a conventional 72-slot 4-pole distributed winding, where the number of slots per pole per phase is 6.

The spiral winding is based on spiral coils, each of which consists of two complementary spirals sharing the same direction, one on the top layer and the other on the bottom layer, connected by vias, as shown in Fig. 1b. It is suitable for high-polarity electric machines. In addition, the PCB winding can be implemented in two different ways. All the coils in a single layer may belong to a single phase or different phases, providing more flexibility for the winding design. Other variants including the rhomboidal coil [11] and the hexagonal coil [12].

The progressive wave winding from [5] shown in Fig. 1c is based on the 8-shaped coil unit. The two coil sides facing each other diametrically are in the same layer. It corresponds to a conventional 12-slot 4-pole distributed winding, whose number of slots per pole per phase is 1.

The continuous wave winding from [4] has two phases placed at two different layers. The number of waves equals that of PM poles, and all traces belonging to the same phase are in

*Dr. Peng Han and Dr. Damien Lawhorn were with the SPARK Laboratory, ECE Department, University of Kentucky, Lexington, KY and they are now with Ansys, Inc., San Jose, CA, USA and Jacobs Engineering, Houston, TX, USA, respectively.

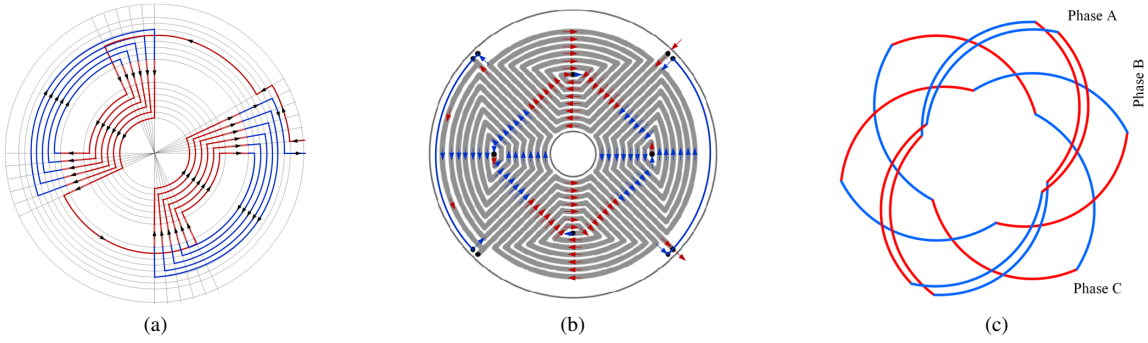


Fig. 1. Typical PCB winding configurations, (a) distributed winding (one phase shown), (b) spiral winding, (c) progressive wave winding (two coil units are shown for phase A and one coil unit is shown for phases B and C). The spiral winding and continuous wave winding are inherently suitable for high-polarity designs.

series. Compared with the other three winding configurations, the continuous wave winding has the simplest structure and thus is a good initial candidate or reference for the design and comparison of PCB stator winding AFPM machines.

This paper presents the systematic optimization and experimental study of a coreless AFPM machines with wave winding PCB stators. The concept of “macro coil” is proposed to model PCB stator windings in order to significantly reduce the computation time of the 3D finite element analysis (FEA) based large-scale design optimization with evaluated winding eddy current losses. The detailed trace-by-trace model was used to check the voltage difference between parallel paths and the resulting circulating currents for a selected design, which has also been fabricated and tested for experimental validation.

The rest of this paper is organized as follows. Section II presents the design and manufacturing considerations of AFPM machines with continuous PCB wave windings. Section III shows the large-scale design optimization workflow and results based on 3D FEA and the macro coil concept, followed by detailed modeling and performance approximation of the selected design. The prototyping and experimental validation are included in Section V and Section VI concludes the paper.

II. AFPM MACHINES WITH PCB WAVE WINDINGS AND DESIGN CONSIDERATIONS

The studied coreless AFPM machine has two surface-mounted PM rotors and a central stator consisting of multiple stacked PCBs, as illustrated in Fig. 2. The PCBs are the same and can be mechanically rotated and mounted to achieve a balanced 3-phase or 2-phase stator. The coil cross section of the wave winding in Fig. 2 shows hundreds of traces that need to be connected in series and parallel to meet the dc bus voltage requirement with the increase of power rating, and at the same time suppress the circulating current introduced by parallel paths.

The dimensions of the copper trace and gaps (horizontal and vertical) between traces depend on the manufacturer and have to be determined before the optimization study. A set of typical dimensions is illustrated in Fig. 3, which leads to an approximate fill factor of 0.2286 considering variations in overall PCB thickness during the manufacturing process.

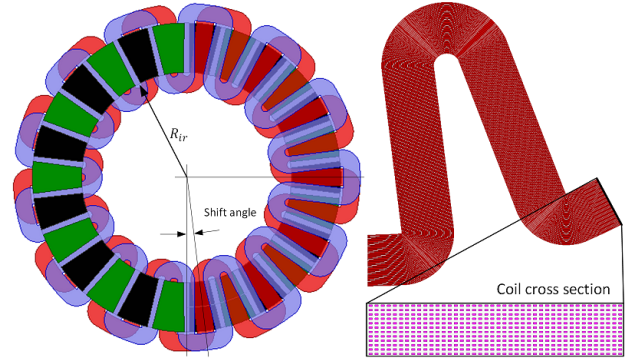


Fig. 2. Coreless AFPM machine with a wave winding PCB stator. A 2-phase PCB stator is illustrated as an example with two PCBs stacked onto each other and shifted by 90 elec. degrees.

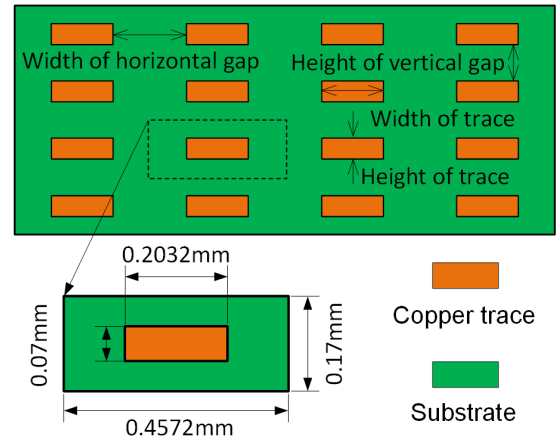


Fig. 3. Cross section of a PCB coil example. There are 16 traces equally spaced in the substrate. Only the envelope geometry, i.e., the macro coil, is modeled in the 3D FEA and trace information is reflected in the fill factor.

III. DESIGN OPTIMIZATION BASED ON 3D FEA AND THE CONCEPT OF “MACRO COIL”

Material properties and magnet dimensions were kept constant during optimization since they are predetermined by available suppliers. Dimensions of the stator and rotor back iron were optimized to achieve the minimum total copper weight and total electromagnetic loss, including the dc winding loss, ac winding loss and PM eddy current loss. Four independent variables were identified for the optimization, as shown in

TABLE I
OPTIMIZATION VARIABLES AND THEIR RANGES.

Variable	Description	Min.	Max.
R_{i_rotor}	Inner radius of rotor [mm]	120	200
$k_{coilwidth}$	Coil width/Max. coil width	0.50	0.95
$k_{rotoryoke}$	Rotor yoke thickness/PM axial length	0.5	1.5
k_{axial_stator}	Stator axial length/PM axial length	0.5	2.0

Table I. All "k_..." variables within the optimization are ratios of that aspect of the motor design with it's limiting maximum bounds.

With the macro coil shown in Fig. 3, the width and height of coils in the large-scale design optimization were constrained to make sure the number of traces fitted in the macro coil is an integer. The equivalent current density, which is the product of the fill factor and real current density in copper traces, was applied uniformly on the cross section of the macro coil for the evaluation of electromagnetic torque, PM eddy current loss, and dc copper loss.

The ac copper loss, i.e., the eddy current loss in copper traces, was estimated using analytical formulas with the sampled flux density variations in the macro coil region instead of the trace-by-trace model. The detailed optimization workflow can be found in [3].

The optimization method is a variation of a 2-level surrogate-assisted algorithm which combines multi-objective differential evolution (DE) and kriging meta-models to accelerate the generation of the Pareto front [14]. This optimization algorithm requires less design evaluations and can be implemented in powerful workstations or high performance computing (HPC) systems to evaluate each 3D candidate design in less than 20 minutes.

Optimization results, including all candidate designs and the Pareto front are shown in Fig. 4. A fitted curve from the obtained Pareto front design set is also plotted to highlight the trade-off between the total electromagnetic loss and copper mass. To achieve a Pareto front as smooth as the fitted curve, more generations should be evaluated. Independent variables in all candidate designs are within their predetermined ranges, as shown in Fig. 5.

A single phase winding with macro coil dimensions of 14.935mm×3.048mm (width×height) was selected as the optimal design with 42 horizontal traces and 12 vertical traces, as visualized in Fig. 6. The optimal 3-phase designs can be achieved following the same optimization approach. For simplicity, the authors derived a 3-phase version by stacking 3 single-phase windings 120 electrical degrees apart, as visualized in Fig. 7. The 3-phase configuration obtained by this approach may not be the optimal design but should suffice for prototyping and experimental validation of the concept and presented analysis methods.

IV. DETAILED MODELING OF PCB STATORS AND PERFORMANCE CHECK

The optimization presented in Section III produces the best tradeoffs between the total loss and total copper weight by

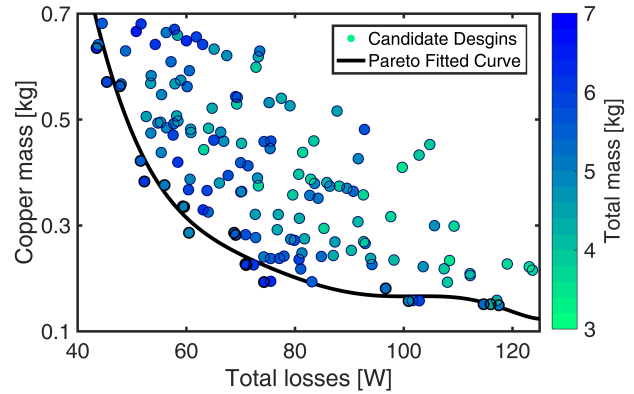


Fig. 4. The Pareto front and all the other designs evaluated by 3D FEA throughout the differential evolution for the 2-phase PCB stator AFPM with wave winding.

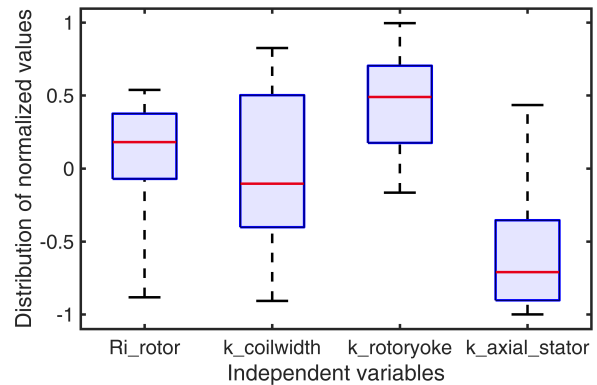


Fig. 5. Distribution of independent variables used within differential evolution optimization. The purple boxes represent the middle 50% of the data points and the red line indicates the median.

evaluating and comparing hundreds to thousands of design candidates using 3D FEA without modeling the copper traces in detail. Detailed trace-by-trace models are used for the final performance check, especially the ac winding losses. Only 1/13 of the machine was modeled by making full use of the symmetry, and a coil of one phase is illustrated in Fig. 8, which has 22.65 million tetrahedral elements and the meshing takes more than 12 hours on the UK HPC system using 2 nodes and 64 cores.

For a 200V dc bus voltage and an assumed modulation index of 0.9, the minimum number of parallel paths is 50

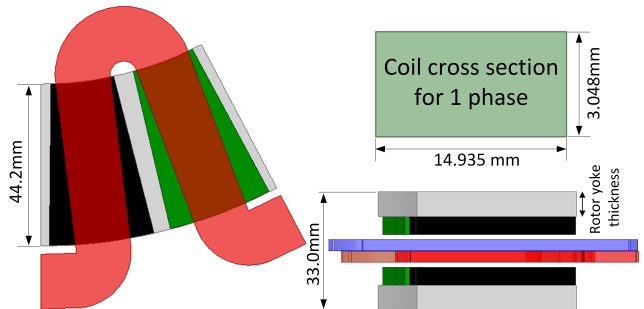


Fig. 6. A single coil of the selected coreless AFPM PCB design. This section represents 1/13th of the full 2 phase design model and the full model's results can be extrapolated through geometry.

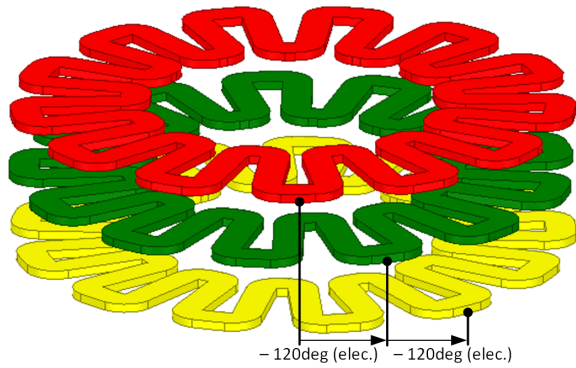


Fig. 7. Wave winding topology PCB stator conductors as implemented within the 3-phase configuration.

according to the overall terminal voltage of 13.6kV with all traces in series. Therefore, the traces within the macro coil were divided into 7 groups (i.e., turns) and each turn has 72 parallel paths. Considering the variation of flux density in the tangential direction is faster than in the axial direction, the 504 traces are grouped in the way illustrated in Fig. 8.

To check the open-circuit (OC) voltage difference between traces and the resulting circulating currents when all traces belonging to the same turn are connected in parallel, the copper traces within turns are numbered in the format of (R, L) as shown in Fig. 9, where R and L denote the number of row and layer, respectively. The flux density distribution for a single pole under the OC condition is shown in Fig. 10.

The OC voltage and peak circulating current of each trace within Turn 7 are visualized by heatmaps shown in Fig. 11a and Fig. 11b, respectively. It can be seen that larger OC voltages occur in layers closer to PMs and rows closer to the coil center line. Consequently, larger peak values of circulating currents mainly appear at regions with high and low OC voltages. With a rotor speed of 3,050r/min, the maximum peak circulating current will be 1.44A, which is almost 4.6 times 0.315A, the peak value of applied current per trace. To make sure that the peak OC circulating current is no larger than the rated applied current, the rotor speed should be limited to 1,400r/min. To achieve higher speeds for this high-polarity coreless machine, new winding configurations that require fewer parallel paths to meet the dc bus voltage requirement or appropriate trace transpositions are desired.

V. PROTOTYPE AND EXPERIMENTAL VALIDATION

To validate the proposed design and analysis, a double-sided coreless AFPM machine with a central stator has been fabricated. The two rotors are the same with 26 surface-mounted NdFeB magnets. Each PCB winding has 6 layers and the bottom layer is used for the returning path. Multiple PCBs can be stacked and rotated to achieve 2-phase or 3-phase designs. A test fixture has been designed and assembled to test the coreless prototype at varying air-gap lengths, rotor numbers, phase numbers, and stator stacking schemes as

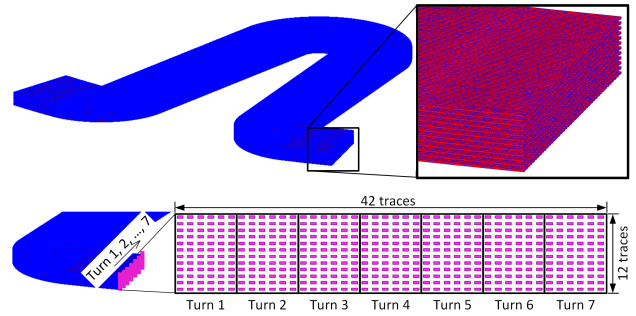


Fig. 8. Meshing of the detailed 3D model for the wave winding PCB stator and a cross section illustration of traces within the macro coil.

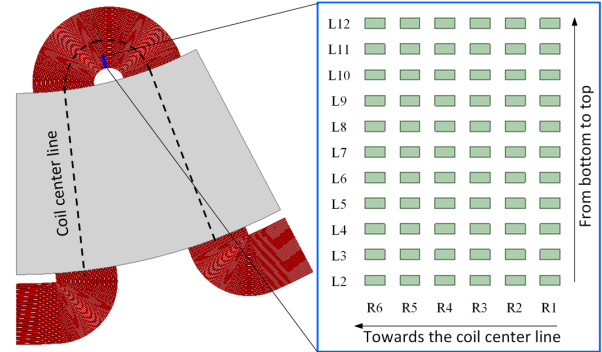


Fig. 9. Cross section of a single turn (Turn 7) of the wave winding PCB stator with 12 vertical layers and 6 columns.

shown in Fig. 12. Dimensions for this prototype PCB coreless AFPM machine are shown in Table II.

The coreless machine was designed to produce a rated torque of 14Nm at 3,050r/min with a fixed dc bus voltage of 300V and a rated phase current of 16Arms. The corresponding rated current density is 10.8A/mm². According to the analysis of the circulating current, the speed has to be limited within 1,400r/min, which means the machine can produce approximately 2.75 horsepower with a reduced requirement for the dc bus voltage. The double-sided configuration shown in Fig. 12 has been tested under the OC condition. The OC back-EMF waveform shown in Fig. 13 is sinusoidal and balanced between

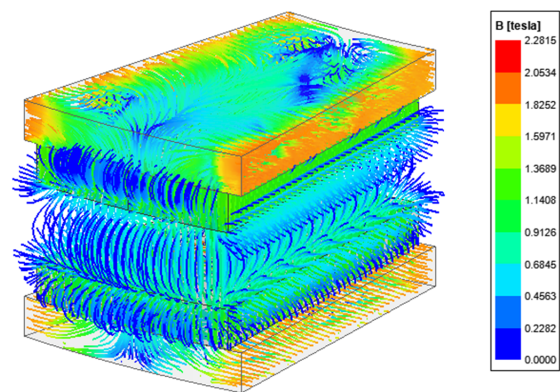


Fig. 10. Flux density distribution in the studied coreless AFPM machine (one pole) with a PCB winding stator.

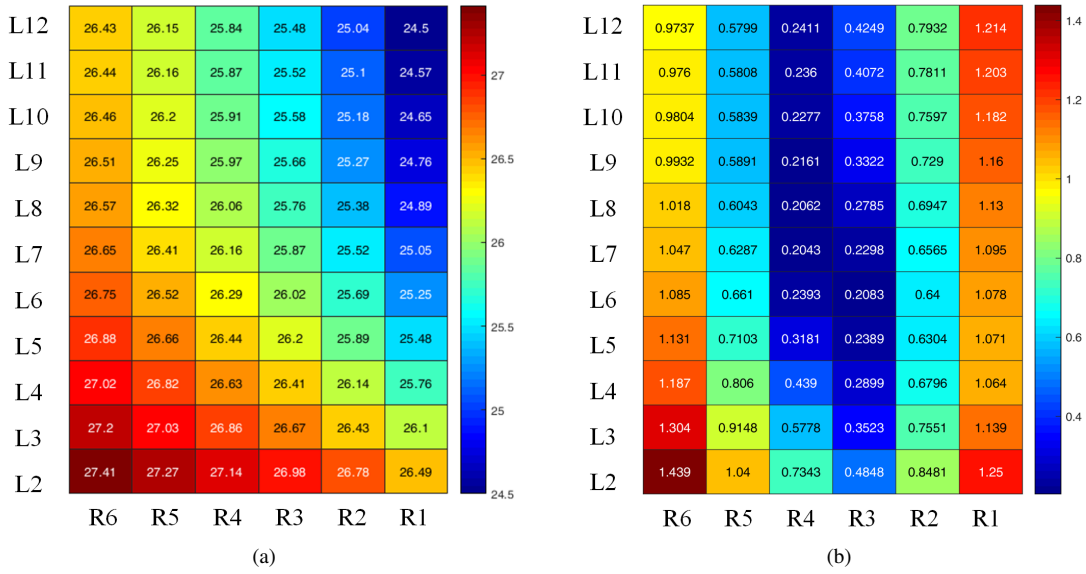


Fig. 11. Electrical performance of Turn 7 of the PCB stator using the detailed trace-by-trace 3D model, (a) OC voltage, (b) peak current.

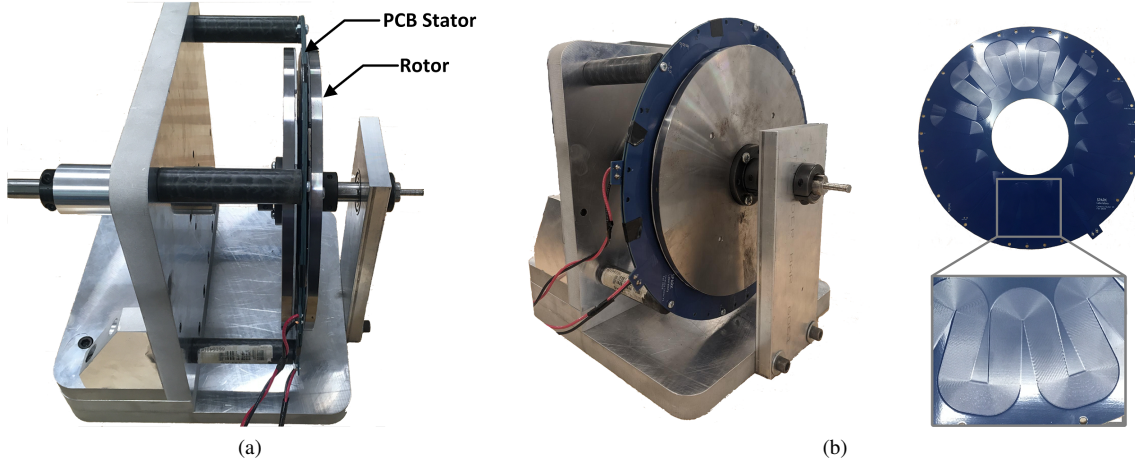


Fig. 12. Experimental setup for the coreless AFPM machine in a 2-phase configuration, (a) the coreless AFPM prototype mounted on the test fixture with a rotor on each side (double-sided configuration), (b) the single-sided configuration mounted on the test fixture and one wave winding PCB.

TABLE II
PROTOTYPE PCB CORELESS AFPM MACHINE DIMENSIONS.

Parameter	Value	Unit
Rotor OD	270.4	mm
Rotor ID	182	mm
Pole pitch at ID	17.2	mm
Pole pitch at OD	28.8	mm
Magnet thickness	5	mm
Back iron thickness	10	mm
Stator ID	144.5	mm
Stator OD	304.9	mm
Trace width/isolation w_t/w_i	0.20/0.025	mm
Trace thickness t_t	0.07	mm
Trace length	8	m
Active layers	5	-

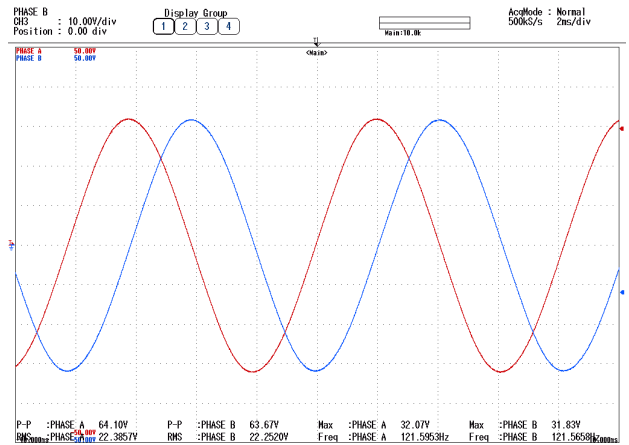


Fig. 13. Experimental OC back-EMF results while operating in two phase mode at 562 r/min and a 1.5 mm airgap .

the two phases. The experimental results for one phase of the two phase AFPM machine closely matches the OC back-EMF of the trace-by-trace model as shown in Fig. 14.

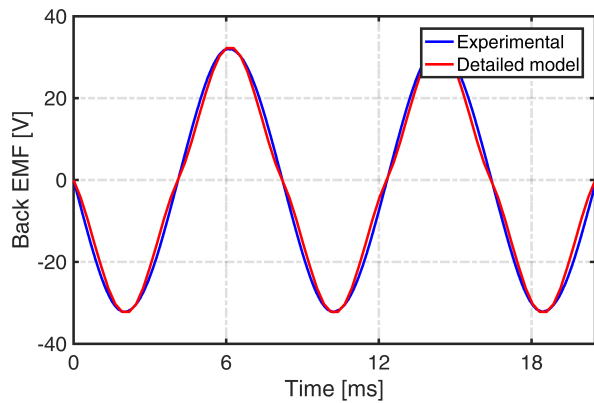


Fig. 14. Single phase comparison of the simulated and experimental OC back-EMF waveforms at 562 r/min.

VI. CONCLUSION

This paper presents a systematic design optimization and experimental study of coreless AFPM machines with wave winding PCB stators. A brief review and comparison of existing PCB winding configurations is conducted first to serve as the starting point of this work and shows the potential of spiral windings and wave windings in high-polarity high-frequency coreless AFPM machines.

The concept “macro coil” is proposed and applied in the large-scale multi-objective optimization to quickly estimate the ac winding losses in each design candidate and reduce the overall computation time. The detailed trace-by-trace model is then built to check the voltage difference between parallel paths and the resulting circulating currents. It has been shown that increasing designed machine power rating of the continuous wave winding stator may cause it to suffer from substantial circulating currents due to the parallel winding traces. To reduce the losses caused by circulating current within PCB stators, alternative winding configurations that can effectively reduce the number of parallel paths or transpose the copper traces are recommended.

ACKNOWLEDGMENT

This material is based upon work supported by the National Science Foundation (NSF) under Grant No. #1809876.

Any opinions, findings, and conclusions or recommendations expressed in this material are those of the authors and do not necessarily reflect the views of the NSF. The support of the University of Kentucky, the L. Stanley Pigman Endowment, of Ansys, Inc., and of Regal Beloit Corp. is also gratefully acknowledged.

REFERENCES

- [1] F. Profumo, A. Tenconi, M. Cerchio, J. F. Eastham, and P. C. Coles, “Axial flux plastic multi-disc brushless PM motors: performance assessment,” in *Proc. IEEE Applied Power Electron. Conf. Expo. (APEC)*, vol. 2, 2004, pp. 1117–1123 vol.2.
- [2] N. Taran, V. Rallabandi, G. Heins, and D. M. Ionel, “Coreless and conventional axial flux permanent magnet motors for solar cars,” *IEEE Trans. Ind. Appl.*, vol. 54, no. 6, pp. 5907–5917, 2018.
- [3] M. G. Kesgin, P. Han, N. Taran, D. Lawhorn, D. Lewis, and D. M. Ionel, “Design optimization of coreless axial-flux PM machines with Litz wire and PCB stator windings,” in *Proc. IEEE Energy Convers. Congr. Expo. (ECCE)*, 2020, pp. 22–26.
- [4] F. Marignetti, G. Volpe, S. M. Mirimani, and C. Cecati, “Electromagnetic design and modeling of a two-phase axial-flux printed circuit board motor,” *IEEE Trans. Ind. Electron.*, vol. 65, no. 1, pp. 67–76, 2018.
- [5] N. S., S. P. Nikam, S. Singh, S. Pal, A. K. Wankhede, and B. G. Fernandes, “High-speed coreless axial-flux permanent-magnet motor with printed circuit board winding,” *IEEE Trans. Ind. Appl.*, vol. 55, no. 2, pp. 1954–1962, 2019.
- [6] M. B. J. Lincoln M. Jore, “Conductor optimized axial field rotary energy device,” U.S. Patent 7109625B1, Sept. 2006.
- [7] H. L. Xiaoyuan Wang and X. Li, “Winding design and analysis for a disc-type permanent-magnet synchronous motor with a PCB stator,” *Energies*, vol. 11, no. 12, 3383, pp. 1–15, 2018.
- [8] D. Gambetta and A. Ahflock, “Designing printed circuit stators for brushless permanent magnet motors,” *IET Electr. Power Appl.*, vol. 3, no. 5, pp. 482–490, 2009.
- [9] R. L. Bernhard L. Schuler and J. Rasmussen, “System and apparatus for axial field rotary energy device,” U.S. Patent 10680479B2, Jun. 2020.
- [10] D. Lawhorn, P. Han, D. Lewis, Y. Chulaee, and D. M. Ionel, “On the design of coreless permanent magnet machines for electric aircraft propulsion,” in *proc. IEEE Trans. Electr. Conf. and Expo (ITEC)*, 2021, pp. 1–6.
- [11] M. . Tsai and L. . Hsu, “Design of a miniature axial-flux spindle motor with rhomboidal PCB winding,” *IEEE Trans. Magn.*, vol. 42, no. 10, pp. 3488–3490, 2006.
- [12] X. Wang, C. Li, and F. Lou, “Geometry optimize of printed circuit board stator winding in coreless axial field permanent magnet motor,” in *proc. IEEE Veh. Power Propul. Conf. (VPPC)*, 2016, pp. 1–6.
- [13] G. Colinet, W. Lamberts, F. Baudart, and B. Dehez, “Investigation on the potential of PCB winding technology for high-dynamic and high-precision linear actuators,” in *Proc. IEEE Energy Convers. Congr. Expo. (ECCE)*, 2020, pp. 3615–3622.
- [14] N. Taran, D. M. Ionel, and D. G. Dorrell, “Two-level surrogate-assisted differential evolution multi-objective optimization of electric machines using 3-d fea,” *IEEE Trans. on Magn.*, vol. 54, no. 11, pp. 1–5, 2018.